Putting unwanted surface states to good use: Large modulation of the superconducting state in a degenerate semiconductor by a gate

Bikash C. Barik,[1,‡] Himadri Chakraborti,[1,2,*] Buddhadeb Pal,[1,3] Aditya K. Jain,[1,4] Swagata Bhunia,[1] Sounak Samanta,[1] Apurba Laha,[5] Suddhasatta Mahapatra,[1] and K. Das Gupta[1,†]

[1] *Department of Physics, Indian Institute of Technology Bombay, Mumbai 400076, India*
[2] *Laboratory of Atomic and Solid State Physics (LASSP), Cornell University, Ithaca, New York 14853, USA*
[3] *Indian Association for the Cultivation of Science, Kolkata 700032, India*
[4] *Dept. of Physics, Royal Holloway, University of London, Egham, Surrey TW20 0EX, United Kingdom*
[5] *Dept of Electrical Engineering, Indian Institute of Technology Bombay, Mumbai 400076, India*

(Received 21 August 2024; revised 23 December 2024; accepted 24 January 2025; published 5 March 2025)

Continuous evolution of superconducting properties as a function of carrier density is difficult to investigate experimentally, unlike the properties of a "gated" semiconductor. This is because superconductors, in general, have carrier densities that are too high for a dielectric insulated gate (as in field-effect transistors) to work. Using an ionic liquid gate, we demonstrate that the modulation of carrier density can alter the superconducting transition temperature by up to 204 mK in epitaxial indium nitride on gallium nitride, accounting for $\geq$10% of the transition temperature in ungated conditions. Our devices are in the metallic regime, in the moderately clean limit ($k_F l \approx 3$–6) throughout the gate voltage range, and their properties are therefore not primarily governed by strong localization, granularity, etc. The primary determinants of the transition temperature in InN, which is a degenerate semiconductor, are carrier density, screening, and interaction, rather than disorder scattering. We show that the observed behavior is consistent with Bardeen-Cooper-Schrieffer s-wave superconductivity, as corroborated by the superconducting parameters we measure. Furthermore, we observe up to 60% suppression of the supercurrent in our experiments. Both positive and negative gate voltages result in suppression of the critical current. Ionic liquid-gated InN thus presents a platform in which s-wave superconductivity can be tuned at low carrier densities, almost 1000–10 000 times lower than in other systems such as niobium nitride. We point out potential areas where low carrier (superfluid) density can find useful applications.

DOI: 10.1103/PhysRevApplied.23.034007

I. INTRODUCTION

The bare interaction between two particles in a many-body system is necessarily modified by the presence of the other particles and excitations. This screening is a function of particle density, which is very difficult to vary in metallic systems. Metals have carrier densities of the order of 10^{23} cm^{-3}, and even a monolayer of metal will have an areal density of at least 10^{15} cm^{-2}. These cannot be modulated by any conventional solid-state gate in a field-effect transistor configuration. This limitation arises because achieving even an approximately 1% change in carrier density demands an unsustainable electric field. Even when using very thin (thickness d) high-K dielectrics, the breakdown field (approximately 1 V/nm) constrains the maximum achievable areal density modulation $\delta n \approx (\epsilon_0 K/e)\,(V_G/d)$ to be of the order of 5×10^{13} cm^{-2}, where V_G represents the gate voltage. In contrast, nondegenerate semiconductor channels offer the flexibility for density modulation due to their significantly lower bulk concentration, typically ranging from (10^{16} to 10^{17} cm^{-3}). This is why semiconductors are "gateable" but superconducting pairing, ferromagnetic exchange, etc., cannot be gate controlled because these usually occur in metals, alloys, or oxides that have carrier densities much higher than approximately 10^{20} cm^{-3}. In recent years, the ionic liquid-gating technique [1–7] has brought ferro- and antiferromagnetic interactions and potential superconducting interactions into the gate-tunable regime [4,8,9] to a certain extent. It is interesting to ask whether an effective attractive interaction between electrons near the Fermi surface can persist in systems with significantly lower electron densities, such as those characteristic of semiconductors (typically in the range 10^{16} to 10^{20} cm^{-3}).

*Contact author: hc2278@cornell.edu
†Contact author: kdasgupta@phy.iitb.ac.in
‡Contact author: bikash.barik@iitb.ac.in

Certain semiconductors, such as GeTe, B-doped diamond, B-doped Si, and InN, do show superconductivity. For instance, InN films exhibit a transition at temperatures $T \sim$ 2–3 K, and in heavily alloyed GeTe, a transition is seen around $T < 0.3$ K [10,11]. Diamond and Si require carrier densities above 10^{21} cm^{-3} for superconductivity [12,13]. Interestingly, the carrier density required for superconductivity in InN is notably lower, falling within the range 10^{17} to 10^{18} cm^{-3} [14–16], which is around 10^3 to 10^4 times less than conventional metals; however, beyond the question of "dressed" electron-electron interactions at lower densities, a lower superfluid density combined with a not-too-low T_c presents significant possibilities. For example, in every current-carrying conductor of length l and cross-sectional area A, the energy (E) has contributions from the magnetic field of the current and the kinetic energy of the charge carriers, commonly referred to as the magnetic (L_M) and kinetic (L_K) inductance, respectively. Here, $E = \frac{1}{2}L_M I^2 + \frac{1}{2}\left(m/ne^2\right) l/(A) I^2$, where L_M depends on the geometrical "configuration" in which the conductor is coiled; however, the second part of the expression depends on the velocity of the current carriers of mass m, charge e, and number density n. Clearly, the resistance (Drude model) of the conductor is $R = L_K/\tau$, where τ is the transport scattering time. It was already noted more than fifty years ago [17] that, while in a normal conductor the kinetic reactance ωL_K can be comparable to R only for frequencies $\omega \approx 1/\tau$, for a superconductor, ωL_K can dominate R at any frequency. Moreover, a low superfluid density would result in a high L_K. In recent literature [18], the significance of low-superfluid-density systems has been pointed out in the context of "fluxonium"-type qubits, where a small Josephson junction is shunted by a large superconducting inductor. The material we have studied, InN, has a carrier density at least 2 orders of magnitude lower than that of NbN_x and granular aluminum, which are commonly used for this purpose.

Another significant use of low superfluid density is in designing superconducting nanowire single-photon detectors (SNSPDs) [19], where the spatial extent of the hotspot depends inversely on the carrier density. The lowest-carrier-density materials used for SNSPDs, tungsten silicides [20–22] still have carrier densities 2 orders of magnitude higher than InN.

It is known that the product of the critical current and the normal-state resistance of a superconducting junction (the $I_c R_N$ product) depends on the superconducting gap on the two sides of the junctions as $\approx \Delta(T = 0)/2e$. Thus, the ability to tune or alter the superconducting gap can enable one to tune the parameters of a Josephson junction with a gate voltage. Indeed, a low carrier density and gate tunability generally go together, for the reasons explained earlier. A change in the superconducting gap would be most simply manifested through a change in T_c. Prospecting for a low-carrier-density and consequently gate-tunable superconductor can thus be a fruitful direction of work.

In this work, through controlled modulation of the carrier density by ionic liquid gating, we achieved a reversible change in the superconducting transition temperature (T_c) by 204 mK with $\pm$3.25 V, corresponding to approximately 10% of the ungated T_c. In these devices, carrier densities were successfully changed by nearly 30% and the critical current by more than 50% compared to their ungated values. The areal capacitance between the gate and the channel was corroborated through independent methods, specifically, Hall-effect measurements and electrochemical impedance spectroscopy (EIS) [7,23]. It is important to note that previous investigations into the field effect in superconductors employed solid dielectric [24] and ferroelectric [25] gates, yielding relatively small effects. More recently, a shift of approximately 80 mK (ΔT_c) was observed in Nb thin films subjected to applied gate voltages ranging from -4 to $+5$ V [26]. On NbN thin films, a ΔT_c of around 85 mK was achieved with applied gate voltages of $\pm$3 V [5,27]. In certain cases, interesting correlations with carrier density has been reported in NbN [28]; however, this was achieved using sets of samples grown under different conditions.

Our prior experiments on angle-dependent critical field [29] revealed that even in epitaxially grown InN films with a thickness of up to 300 nm, superconducting electrons are inherently confined to a surface layer with a thickness of $d_s \sim 25$ nm, a dimension smaller than the coherence length ξ_0. Additionally, the significant density of surface states pins the surface Fermi level within the conduction band, eliminating the presence of a Schottky barrier at the surface and, concurrently, making hole doping of the material exceptionally challenging [30]. The surface states of InN are thus often considered problematic, as they prevent its use as a narrow-gap semiconductor; however, it is precisely this combination of low bulk carrier density and the potential for a substantial response to perturbations in the surface states that renders InN an intriguing candidate for ionic-liquid gating, where the strongest perturbation occurs close to the surface and gradually diminishes within a few Thomas-Fermi screening lengths as one moves into the bulk of the material.

II. EXPERIMENTAL SECTION

The InN samples were grown on c-oriented sapphire substrates by plasma-assisted molecular beam epitaxy (PA-MBE) [29,31–33] with negligible oxygen impurities, as demonstrated by the absence of oxygen O1s core level transition in x-ray photoemission spectroscopy results [33]. Patterned channels [Fig. 1(a)] on these samples were lithographically fabricated using Al_2O_3 as a hard-mask layer followed by chlorine-based dry etching and subsequent removal of the hard mask by HF. The devices each had an effective channel area of $1150 \times 100\ \mu m^2$ and a thickness of approximately 300 nm [Fig. 1(b)]. Layers of Au and Ti (80 and 20 nm, respectively) were used for the source (S) and drain (D) contacts. The gate electrode is much larger in area than the channel, eliminating the necessity for a reference electrode [7]. We used diethylmethyl(2-methoxyethyl)ammonium bis(trifluoromethylsulfonyl)imide (DEME-TFSI) as the ionic liquid (IL). The contacts were covered with silicone gel during application of the IL (see Appendix A for the detailed fabrication steps). The ionic liquid was cured under high vacuum at 110 °C for around 48 h. All low-temperature measurements were carried out in a vacuum of 10^{-5} mbar or better. Figure 1(c), shows typical output characteristics (i.e., V_{SD} vs I_{SD} measurements) at different gate voltages (V_G), ranging from +0.8 to −0.8 V with a step increment of 0.2 V. The gate leakage remained 10^3 times smaller than I_{SD}. The observed trends and Hall-voltage measurements at 300 K (as well as at 4.8 K), confirm that the carrier density is stable and indeed changes in a predictable way, allowing clear determination of the electron density (n) and mobility (μ_e) from four-terminal measurements. We recorded an approximately 30% change in carrier density with applied gate voltage, a finding of considerable relevance within the context of high-carrier-density systems [4,6,34,35].

At a temperature of 300 K, we observed $\mu_e \sim 220\ \mathrm{cm^2\,V^{-1}\,s^{-1}}$ at $V_G = 0$ V, yielding a mean free path $l \approx 10$nm (see Table I). The capacitance determined from our measurements—approximately $8.8\ \mu\mathrm{F\,cm^{-2}}$, as depicted in Fig. 2(b)—surpasses what is achievable in metal-oxide-semiconductor field-effect transistors or high-electron-mobility transistors. All low-temperature measurements were performed below the glass transition temperature (T_G) of the ionic liquid (refer to Appendix C for the behavior of an ionic liquid gate). It is crucial to note that changing the gate voltage will have the desired effect only if done at $T \gg T_G$. In our experiments, we always allowed the sample to warm up to room temperature for setting V_G.

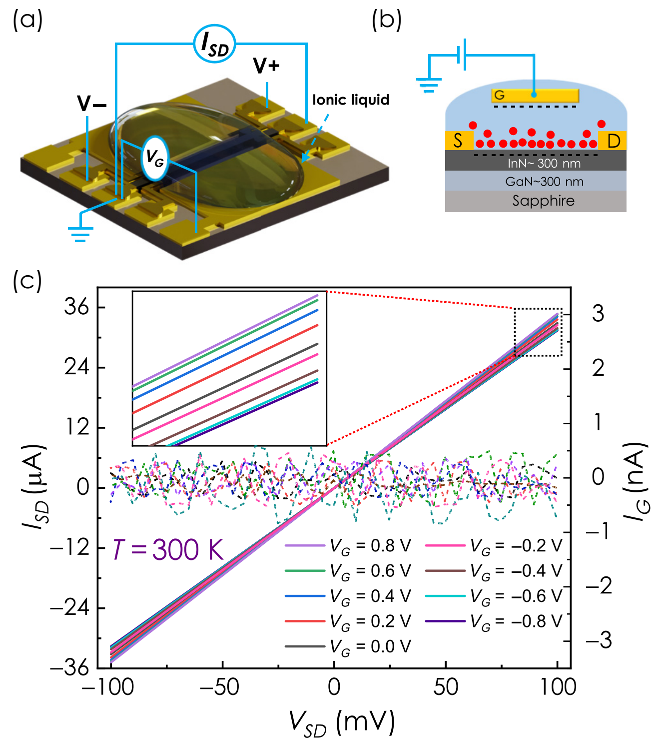

FIG. 1. Electric double-layer transistor and output characteristics. (a) Schematic diagram of InN-IL-gated transistor. The area of the gate electrode is much larger than the channel area (see explanation in text). DEME-TFSI ionic liquid is used. (b) Cross-sectional view. (c) Output characteristics at room temperature. The inset shows a clear shift in current values with applied gate voltage. Gate leakage currents are shown in the right-hand panel. These data are taken from an InN-B3601 sample.

III. RESULTS AND DISCUSSION

The superconducting critical temperature was measured in InN devices subjected to ionic liquid gating. The findings presented here are from two devices, B3601 and B3603 (from two different wafers), demonstrating tunable superconducting parameters with variations in T_c of 204 and 105 mK, as shown in Figs. 3(a) and 3(b), respectively. The transition temperature of InN is primarily governed by carrier density rather than disorder scattering ($k_F l$) [36,37]. It has to be noted that we are able to both enhance and suppress the T_c in the same device. This cannot be explained by assuming a thin perturbed layer near the surface and a relatively unperturbed bulk superconductor in parallel. In such a case, the resistive T_c can be enhanced by a surface layer with a higher T_c "short circuiting" the bulk, but it cannot be suppressed by a layer with a lower T_c, since the bulk superconductor would then act as a shorting path. Furthermore, we see no evidence of a two-step resistive transition that would indicate the presence of two parallel conducting layers. The perturbation of the superconducting state that we see is thus likely to be a state spanning the entire superconducting region.

We find reasonable agreement of the measured variation of the superconducting parameters with the expectations from an s-wave Bardeen-Cooper-Schrieffer (BCS) superconductor having a simple free-electron (density n) Fermi surface. The zero-temperature coherence length for a BCS s-wave superconductor is [38]

$$\xi(0) \approx \frac{\hbar v_F}{\pi \Delta(0)}, \tag{1}$$

where $v_F = \hbar/m\left(3\pi^2 n\right)^{1/3}$ is the Fermi velocity and $\Delta(0) \propto T_c$ is the superconducting energy gap at $T = 0$.

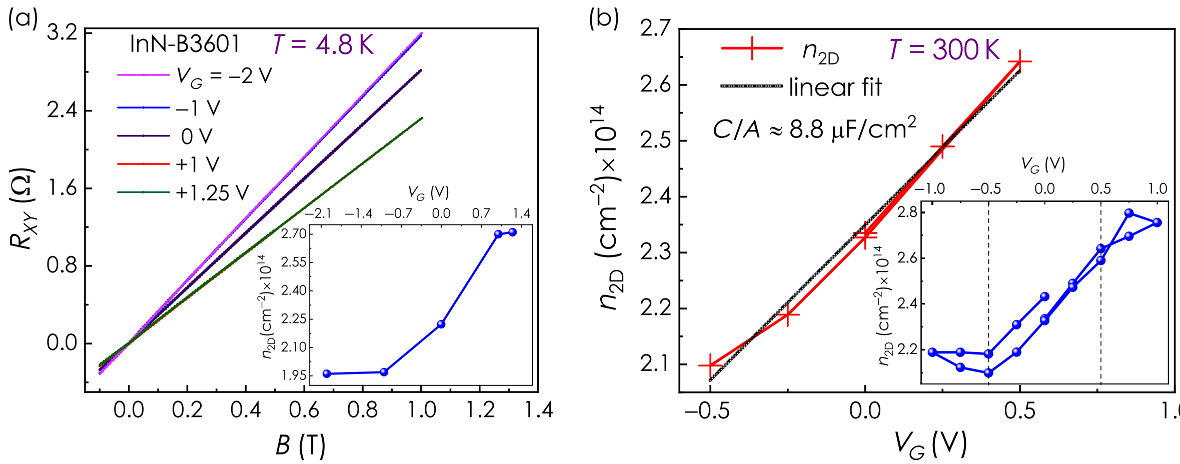

FIG. 2. Hall measurements. (a) Hall voltage data at $T = 4.8$ K. The carrier density modulation is shown in the inset. (b) Measured capacitance from the data over a range of gate voltages (V_G) spanning ±0.5 V.

The coherence length should vary as

$$\frac{\delta\xi}{\xi(0)} \approx \frac{1}{3}\frac{\delta n}{n} - \frac{\delta T_c}{T_c}. \tag{2}$$

The value of $\xi(0)$ can be conveniently calculated from the critical field data (Fig. 4); the carrier density and T_c are directly measured. This relation thus gives a good check on the consistency of the measurements that does not require the exact constant of proportionality between $\Delta(0)$ and T_c to be known. The calculated and measured values of $\delta\xi/\xi(0)$ agree within a factor of 2, which can be attributed to the disorder correction arising from a relatively small mean free path $l \approx 10$ nm, which forces the observed ξ to reduce to $\xi_{\text{obs}} \approx 0.85\sqrt{\xi(0)l}$ [39]. Given that we have $l \sim 10$ nm $\ll \xi(0)$, a correction of the order of what we observe is certainly expected; however, given that $k_F l \gg 1$, we do not expect any strong localization effects or significant granularity effects. This is also supported by hysteresis-free *IV* characteristics in the critical current measurements, as shown in Fig. 5. If internal Josephson junctions arising from several grain boundaries were a dominant factor, significant hysteresis would have been expected.

We thus consider free-electron estimation of the density of states of at the Fermi level, $N(0) = m/\pi^2\hbar^2\left(3\pi^2 n\right)^{1/3}$, to be reasonable. This can be used to infer the variation of the strength of the attractive interaction V, near the Fermi surface via the determination of $\lambda = N(0)V$ by inverting the Eliashberg-McMillan equation,

$$T_c = \frac{\Theta}{1.45}\exp\left(\frac{-1.04(1+\lambda)}{\lambda - \mu^*(1+0.62\lambda)}\right), \tag{3}$$

TABLE I. Bulk carrier density (n_{3D}), density of states at the Fermi level ($N(0)$), superconducting transition temperature (T_c), Fermi velocity (v_F), mean-free path (l), Ioffe-Regel parameter ($k_F l$), electron-phonon coupling strength (λ), coherence length (ξ), and Maki parameter (α) are obtained from two devices, namely InN-B3601 and InN-B3603. The carrier densities were obtained from direct measurement of the Hall resistance (Fig. 2). The transport mean free path was calculated from four-terminal longitudinal resistance in the same Hall bar. The coherence lengths were calculated from direct measurement of the perpendicular critical field. Quantities like v_F, $k_F l$, and $N(0)$ were calculated using a free-electron model. The calculation of λ and the Maki parameter were conducted using the Macmillan equation [Eq. (3)] and Werthammer-Helfand-Hohenberg theory, respectively.

Sample	V_G (V)	n_{3D} (m^{-3})	$N(0)$ (m^{-3}/eV)	T_c (K)	v_F (m/s)	l (nm)	$k_F l$	λ	ξ (nm)	α
B3601	−2	6.53×10^{24}	7.69×10^{26}	2.177	6.68×10^5	9.07	5.24	0.44229	38.82	0.0767
	−1	6.56×10^{24}	7.71×10^{26}	2.174	6.69×10^5	9.30	5.38	0.44215	39.09	0.0745
	0	7.41×10^{24}	8.02×10^{26}	2.146	6.97×10^5	9.84	5.93	0.44090	40.73	0.0699
	+1	9.00×10^{24}	8.56×10^{26}	2.087	7.44×10^5	9.52	6.12	0.43844	42.76	0.0649
	+1.25	9.03×10^{24}	8.57×10^{26}	2.072	7.45×10^5	9.35	6.02	0.43779	43.06	0.0647
B3603	−3.25	5.11×10^{24}	7.09×10^{26}	2.074	6.15×10^5	6.15	3.27	0.43788	31.8	0.1214
	0	6.82×10^{24}	7.80×10^{26}	2.012	6.78×10^5	8.60	5.03	0.43519	37.2	0.0949
	+0.5	7.07×10^{24}	7.90×10^{26}	2.004	6.86×10^5	8.26	4.90	0.43484	37.4	0.0937
	+3.25			1.870				0.42887		

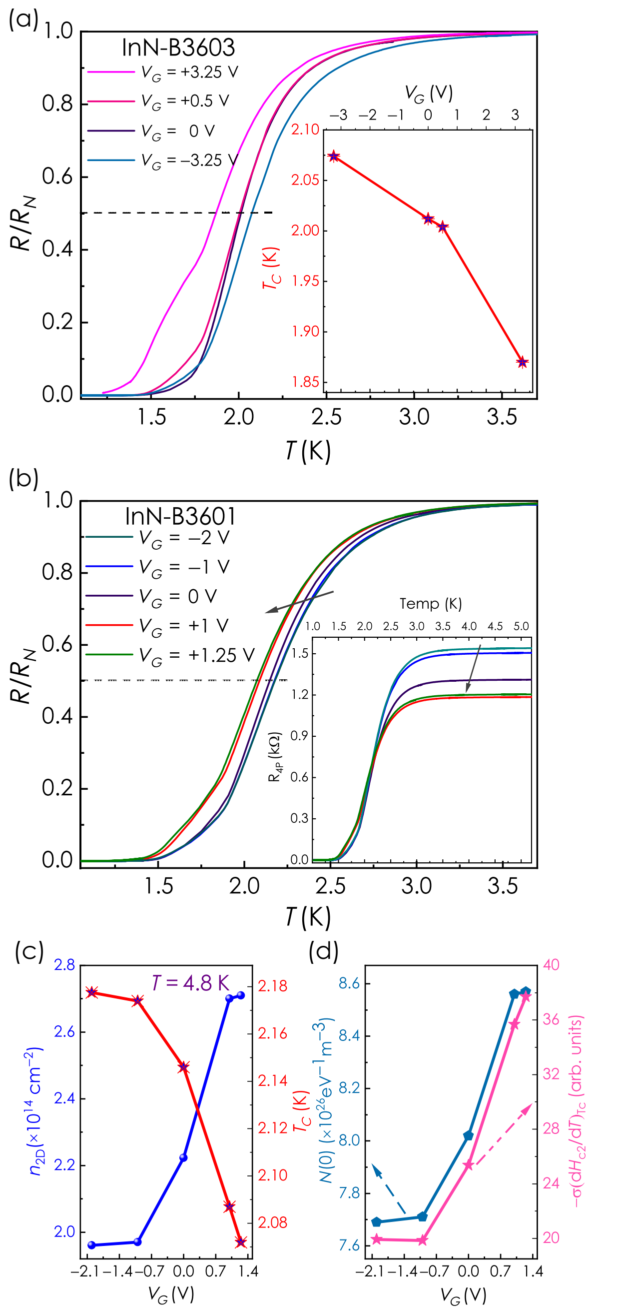

FIG. 3. Critical temperature (T_c) measurements. (a) Normalized R–T plots for different applied gate voltages for the InN-B3603 sample. The inset displays the corresponding superconducting T_c measured at various gate voltages, revealing an estimated value of $\Delta T_c = 204$ mK within the voltage range ±3.25 V. The dashed line (at 0.5) is the reference at which the resistance becomes half of the normal resistance ($R_N/2$). (b) Normalized R–T plots for different gate voltages for the InN-B3601 sample. The data shown in the inset are not normalized. (c) Carrier densities and corresponding superconducting transition temperatures for different gate voltages. Carrier densities were measured at $T = 4.8$ K (above the superconducting transition temperature). (d) Estimation of density of states from the free-electron-theory relation (left axis) and the dirty-limit relation (right axis).

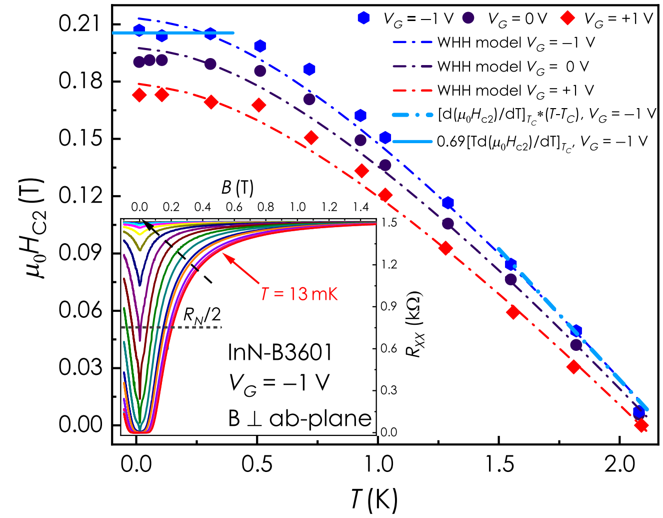

FIG. 4. Critical field (H_{c2}) measurements. Temperature dependence of critical field under various applied gate voltages, fitted with the Werthammer-Helfand-Hohenberg model.

where $\mu^* \approx 0.1$ is the Coulomb pseudopotential [40], which accounts for the electron-electron repulsive interaction, and $\Theta \approx 370$ K is the Debye temperature [41]. The coupling constant found here ($\lambda < 1$) suggests that InN behaves like a weak-to-medium-coupling superconductor. Clearly, at lower carrier densities, the pairing interaction strength gets stronger, resulting in a higher T_c, as depicted in Fig. 3(c). The zero-temperature coherence lengths $\xi(0)$ calculated from the extrapolated values of the critical field (Table I) also mirror this increase of T_c, showing that the superconducting state is stronger at lower carrier densities.

Furthermore, it is known that the density of states is proportional to the slope of the upper critical field [28,42,43], i.e.,

$$N(0) \propto -\sigma \left(\frac{dH_{c2}}{dT}\right)_{T_c}. \qquad (4)$$

The calculated $N(0)$ is shown in the right-hand panel of Fig. 3(d) and compared with the free-electron values $N(0) = m/\pi^2\hbar^2 \left(3\pi^2 n\right)^{1/3}$, exhibiting a very good agreement.

Next, we looked into the temperature dependence of the critical field. The magnetic field value (normal to the surface) at which the resistance of the superconductor attains half of its normal state value (the mean field value) is taken as the critical field (H_{c2}). Curves of $H_{c2}(T)$ were fitted using the well-known Werthammer-Helfand-Hohenberg (WHH) model [43,44] to understand the role of spin-orbit coupling, if present in the system, on the superconducting phase. The WHH model gives the following

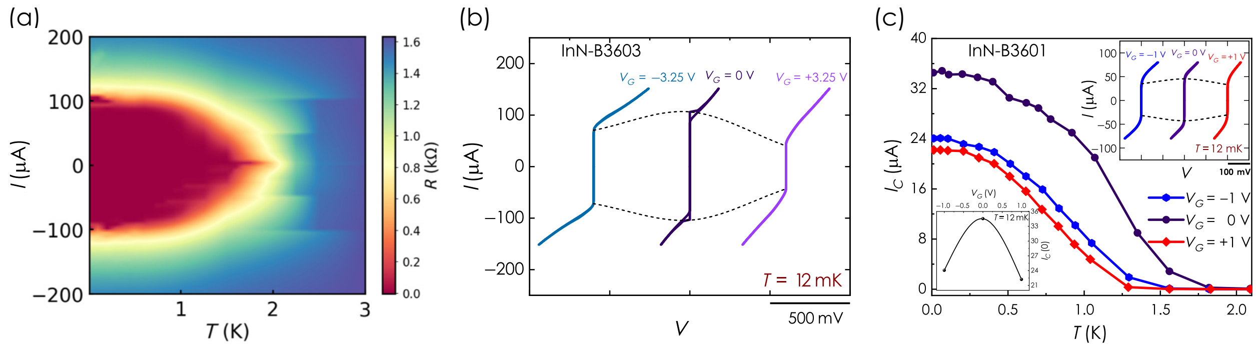

FIG. 5. Critical current (I_c) measurements. (a) Critical current measurements for $V_G = 0$ V for an InN Hall bar. (b) The measured values of the critical current (I_c) exhibit suppression for both positive and negative applied gate voltages for the InN-B3603 sample. (c) Temperature-dependent measurements of the critical current (I_c) for the InN-B3601 sample exhibit bipolar suppression of I_c, as shown in the inset.

equation:

$$\ln\left(\frac{1}{t}\right) = \sum_{\nu=-\infty}^{\infty}\left(\frac{1}{|2\nu+1|} - \left[|2\nu+1| + \frac{b_c}{t} + \frac{(\alpha b_c/t)^2}{|2\nu+1| + (b_c+\lambda_{so})/t}\right]^{-1}\right), \quad (5)$$

where $t = T/T_c$, $\alpha = 3/2mv_F{}^2\tau$ is the Maki parameter, the dimensionless magnetic field $b_c = \mu_0 h_c = e\hbar/2m\pi\alpha(\mu_0 H_{c2})/(k_B T_c)$, and λ_{so} is the spin-orbit scattering constant. The analysis reveals a small Maki parameter $\alpha < 0.1$ and virtually no impact of the spin-orbit term within the measured range of carrier densities (see Table I). This is further confirmed by evaluating the limiting orbital field, H_{c2}^{orb}, using the expression $H_{c2}^{orb}(T=0) \approx 0.7|T(dH_{c2})/(dT)|_{T_c}$. The calculated values closely correspond to the experimental data, as demonstrated for a gate voltage of $V_G = -1$ V (sky-blue line) in Fig. 4. In cases where spin-orbit coupling is strong, one obtains a high value of the Maki parameter (approximately 2–3), as observed in our earlier work [45].

There is, however, one significant aspect in which an indicator of the strength of the superconducting state follows an opposing trend. In general, the Landau-Ginzburg calculation of the critical current (I_c) of a thin film [39] would predict a variation $I_c(T) \propto 1/\xi(T)$ and hence approximately increase with $\sqrt{H_{c2}}$. In bulk superconducting wires, too, when the magnetic field created by the current reaches the critical field at the surface, global superconductivity breaks down; however, we find that the application of a gate voltage, either positive or negative, substantially suppresses the critical current by as much as 60% [see Fig. 5(b)]. Many recent experiments have demonstrated gate-controlled critical-current suppression in superconducting films [46–50]. A set of experiments suggest that critical-current suppression is occurring due to Cooper-pair breaking induced by the gate field [47,49,50]. Most likely, this effect is due to modification of the electron distribution in the channel in response to the additional electric field arising from the gate. It is possible that the wavefunction, as it either gets pulled toward the surface or pushed into the nonsuperconducting bulk region, in fact encounters regions with a smaller normal-state mean free path. This, in turn, leads to increased surface scattering and granularity effects, leading to the suppression of the critical current.

IV. CONCLUSION

This study demonstrates the significant potential of ionic liquid gating in modulating the superconducting properties of indium nitride (InN), a degenerate semiconductor. By precisely controlling the carrier density, we achieved a reversible variation in the superconducting transition temperature of approximately 204 mK, corresponding to a modulation 10% of the ungated T_c. Critical-current suppression of up to 60% was also observed for both positive and negative gate voltages, highlighting the ability of gate voltages to comprehensively influence superconducting parameters.

Our findings indicate that superconducting behavior in InN is governed primarily by carrier density rather than disorder scattering, consistent with the characteristics of a BCS s-wave superconductor. The ability to tune superconductivity at significantly lower carrier densities compared to conventional systems such as NbN establishes InN as a promising material for low-carrier-density superconducting applications, including quantum devices such as fluxonium qubits and superconducting nanowire single-photon detectors.

Additionally, the ability to modulate carrier density and alter intrinsic parameters in a controlled manner opens new avenues for exploring quantum phase transitions in low-dimensional systems [51–54]. Such systems are crucial for understanding emergent phenomena, including unconventional superconductivity, superconductor-insulator transition, and non-Fermi-liquid behavior, among others.

These results not only highlight the versatility of ionic liquid gating but also underscore the utility of leveraging surface states—which are often considered detrimental—for advanced functionalities in superconducting materials. Future exploration of broader density modulation and interaction-driven phenomena could unlock further opportunities for device engineering in low-dimensional and quantum materials.

ACKNOWLEDGMENTS

We acknowledge support from the Department of Science and Technology, Government of India, under project RD/0120-DSTIC01-001, and the Science and Engineering Research Board (SERB), Government of India, under project CRG/2018/001405. B.C.B. acknowledges financial support through the DST-INSPIRE fellowship of the Government of India. We thank Amit P. Shah (TIFR, Mumbai) for his assistance with the dry-etch process and Professor Saibal Sarkar (Department of Energy Science and Engineering, IIT Bombay) for providing access to deposit Al_2O_3 films. We thank Dr. Parushottam Majhi for useful discussions and Mr. Debashish Shah for assistance with several measurements.

APPENDIX A: INDIUM NITRIDE SAMPLE FABRICATION PROCESS

Here, we give a detailed description of the growth technique, fabrication processes, and different characterization techniques for the InN samples (Fig. 6) that we used in our experiments. The InN samples were grown in a PA-MBE system (RIBER Compact 21) with RIBER Addon rf plasma source for the active N species on sapphire substrates, and this growth was conducted by Kankat Ghosh and Swagata Bhunia [33]. The first GaN layer of approximately 300 nm is grown on the sapphire substrate, and then approximately 300 nm InN is grown on top of that. To make the channel of InN, etching is required. The sample goes through different stages during fabrication, and these are outlined below.

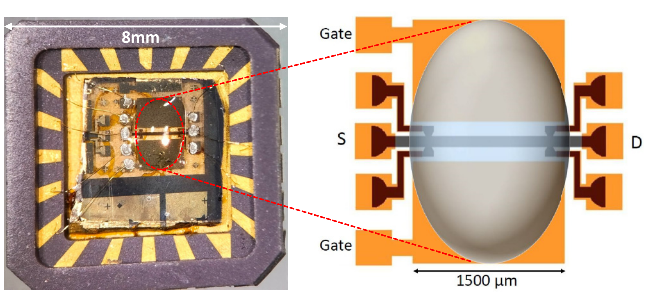

FIG. 6. Actual InN device. The region in which the ionic liquid is deposited is shown by the red-dashed line on the right, and a schematic diagram of the device is shown on the right.

1. Fabrication steps

The fabrication steps are described below.

(1) Substrate preparation: cleaning of the sample with acetone and isopropyl alcohol.

(2) Deposition of 100 nm Al_2O_3 as a hard mask using atomic-layer deposition.

(3) Production of Hall-bar pattern by photolithography. This includes:

(a) Spin coating using S1813 positive photoresist.

(b) Exposing to UV light through a mask using a mask aligner (MA400).

(c) Development in MF319 developer solution.

(4) Etching Al_2O_3 in HF solution.

(5) Dry etch of InN in reactive etching system (RIE).

(6) Removal of photoresist and Al_2O_3.

(7) Patterning contacts by photolithography.

(8) Metal deposition by thermal evaporation, with thicknesses of 20 and 80 nm for Ti and Au, respectively.

(9) Liftoff in acetone.

(10) Mounting in a leadless chip carrier and bonding using a wire bonder.

(11) Deposition of ionic liquid on the Hall bar and curing for 48 h at high vacuum (pressure $< 1 \times 10^{-5}$ mbar) and at temperature 110 °C.

APPENDIX B: TRANSISTOR CHARACTERISTICS

Figure 7 shows the transfer characteristics of the IL-gated InN at room temperature. To maintain a constant source-drain voltage (V_{SD}) of 100 mV, a dc voltage source is used. The gate voltage (V_G) is swept in 0.1-V steps using another voltage source. Notably, different settling times—ranging from 30 to 240 s—are set during the gate-voltage sweep. These settling times allow for the system to stabilize after voltage changes. The measured value of the gate leakage current is approximately 3 orders of magnitude smaller than the source-drain current. This substantial difference ensures that gate leakage does not impact the device's performance. The observed trend in the data indicates n-type characteristics, as I_{SD} increases with the application of increasingly positive V_G.

APPENDIX C: BEHAVIOR OF AN IONIC LIQUID GATE

Figure 8 shows the striking difference between the behavior of an ionic liquid gate and a conventional dielectric gate. The ionic motion within the liquid starts to undergo a slowdown below approximately 230 K. Furthermore, below a specific temperature, marked as the glass transition temperature (T_G), the ions associated with the

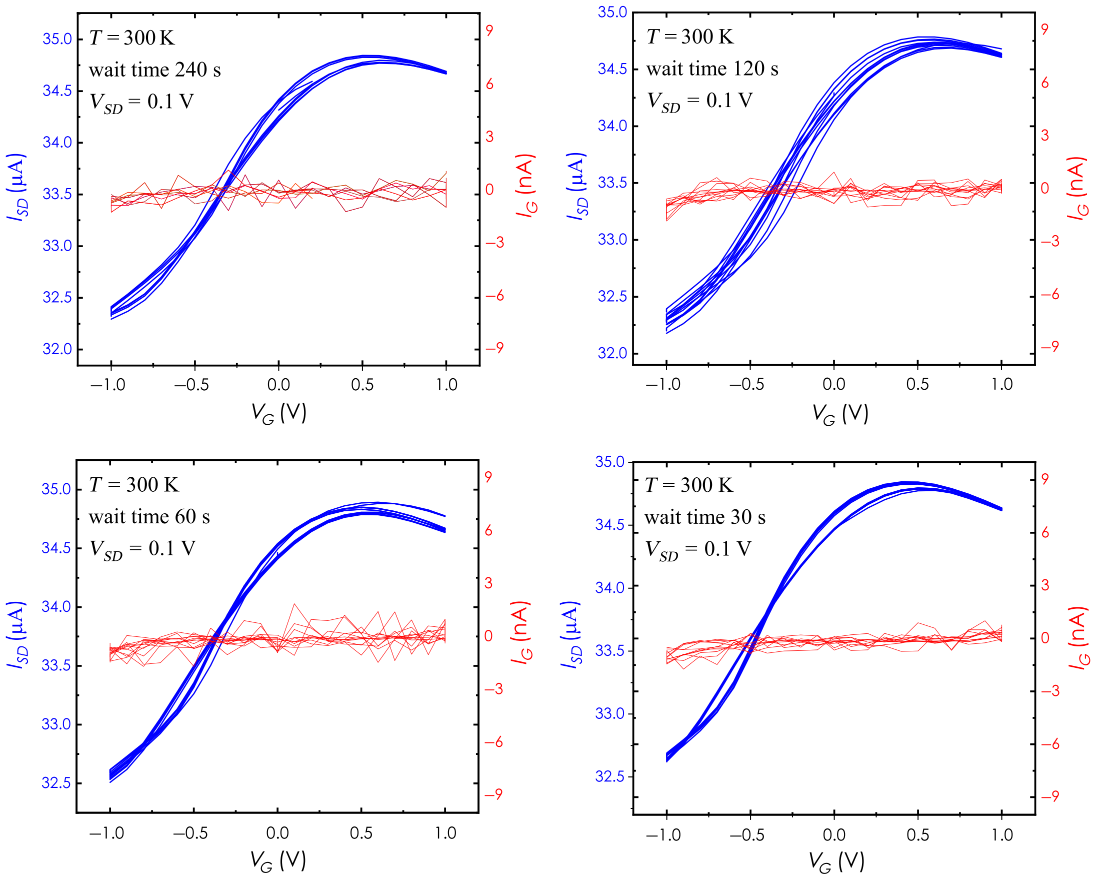

FIG. 7. At $T = 300$ K, the transfer characteristics exhibit a nearly hysteresis-free nature across various settling times (InN-B3601 sample).

ionic liquid experience complete immobilization [23,55,56]. A gate voltage $V_G = -1$ V was applied, and the sample was cooled down to 10 K. The resistance follows the blue curve. The corresponding gate leakage current is illustrated in the inset. At 10 K, the voltage source is set to zero and disconnected. The sample is then allowed to warm up, but it continues to behave as if the gate voltage is still present. When the glass transition temperature (T_G) is reached, the ions in the ionic liquid regain their motion and adjust to the absence of the external field. At this point, one begins to see considerable fluctuations in the gate leakage current. This happens over a range of $T \approx 180$–200 K, which corresponds well to the known T_G value of DEME-TFSI. Changing the gate voltage will have the desired effect only if done at $T \gg T_G$. In our experiments, we always allowed the sample to warm up to room temperature for setting V_G.

APPENDIX D: CAPACITANCE MEASUREMENTS

1. From gate response

The time response of the electrical double layer (EDL) gate in the InN film to a step change in gate bias voltage (V_G) was investigated, and the results are illustrated in Fig. 9, which depicts the growth and decay curves for various gate voltages.

The plots in Fig. 9 show the time response of the InN film resistance to negative gate voltages, revealing distinct growth and decay curves. The time scale for capacitor charging and discharging is extracted from these curves. Notably, for $V_G = -0.5$ V, the fast time scale (τ) is found to be consistent for both the growth (6.9 s) and decay (9.5 s) processes, indicating the charging and discharging of the EDL. The gate leakage current suggests that gate charging occurs through an equivalent resistance (R_G) of approximately 700 MΩ.

The time constant of the charging and discharging curves ($\tau = RC$) is used to determine the gate capacitance (C_G). For $V_G = -0.5$ V, the calculated gate capacitance is approximately 8.52 μF/cm^2. A similar analysis for $V_G = -1$ V yields a gate capacitance of around ~ 10.4 μF/cm^2, with gate charging occurring through an equivalent resistance of $R_G \simeq 400$ MΩ, as depicted in Fig. 9. The gate capacitance values measured by this technique match well with the capacitance derived from Hall measurements, i.e., 8.8 μF/cm^2 (see main text).

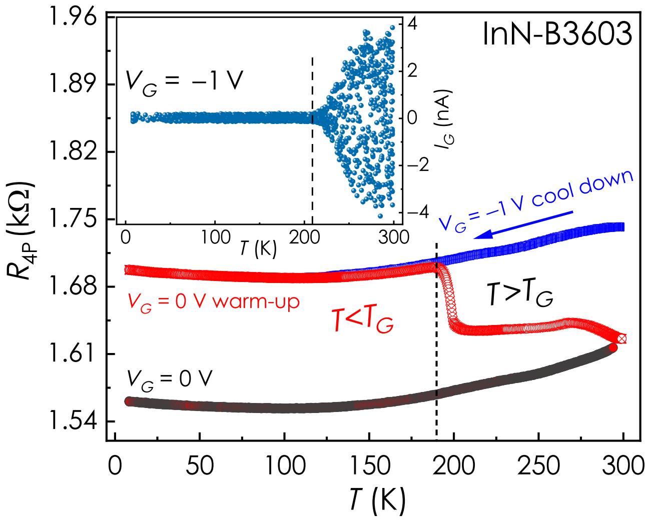

FIG. 8. The glass transition temperature phenomenon is investigated by applying a gate voltage of $V_G = -1$ V and subsequently removing the gate voltage at a low temperature of 10 K. The resulting observation of a significant jump in resistance serves as a clear indicator of the glass transition temperature associated with the ionic liquid. The inset depicts the recorded gate leakage current at $V_G = -1$ V, providing a compelling illustration of the phenomenon associated with the freezing of ions.

2. From electrochemical impedance analysis

We used electrochemical impedance spectroscopy to study the frequency-dependent impedance and to measure the EDL capacitance [2,4]. We measure the impedance of gated InN thin films as a function of frequency for different applied gate voltages from 37 mHz to 2 kHz. Impedance measurements are performed using two lock-in amplifiers. The low-frequency measurement is conducted by configuring a high time constant of 30 s and a corresponding settling time of 300 s. The gate voltage is applied using

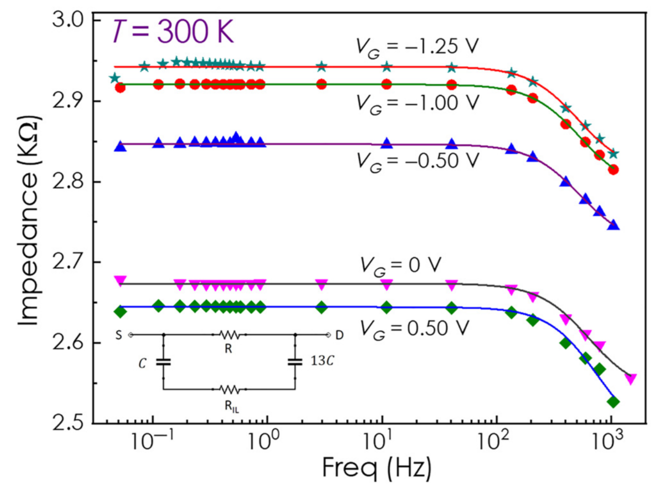

FIG. 10. (a) Frequency-dependent impedance of InN thin film at different gate voltages. The solid lines are the fits obtained using the circuit models shown in the inset. Here, R and R_{IL} are the resistances of the sample and ionic liquid, respectively.

a voltage source. Lock-in amplifiers do not give the value of impedance directly, but it can be calculated using the following relations:

$$Z = \frac{V_S}{I_S} = \frac{V_S}{V_R} \times R = R \times \left(\frac{V_S' + jV_S''}{|V_R|} \right), \tag{D1}$$

$$Z = R \times \left(\frac{V_S' + jV_S''}{\sqrt{(V_R')^2 + (V_R'')^2}} \right), \tag{D2}$$

$$Z' = R \times \frac{V_S'}{\sqrt{(V_R')^2 + (V_R'')^2}}, \tag{D3}$$

$$Z'' = R \times \left(\frac{V_S''}{\sqrt{(V_R')^2 + (V_R'')^2}} \right), \tag{D4}$$

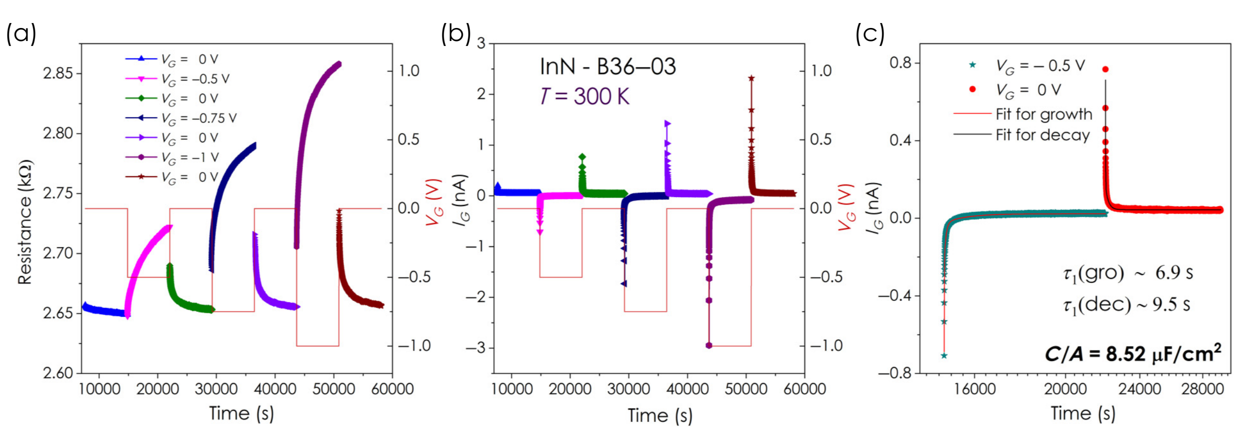

FIG. 9. (a) Transient response of InN film resistance to negative gate voltages, with the gate leakage currents corresponding to these gate voltages shown in (b). (c) Transient response of the gate leakage current for $V_G = -0.5$ V. The value of the capacitance calculated from the fitting is also shown.

TABLE II. Capacitances and resistances of ionic liquid for different applied gate voltages obtained from EIS.

V_G	Capacitance ($\mu F/cm^2$)	R_{IL} (kΩ)
0.5	4.84	38.6
0	4.5	50
−0.5	4.4	61.8
−1	4.33	61.9
−1.25	4.45	62.6

where V_S and V_R are the voltages across the InN sample and a standard 1 kΩ resistor, respectively. The latter is used to measure the current through the sample. Additionally, Z' and Z'' are the real and imaginary parts of the impedance, and Z is the total impedance of the system. The model shown in the inset of Fig. 10 is the capacitive coupling between InN film with resistance R and the ionic liquid with resistance R_{IL}. A constant current of 10 μA is applied by supplying 2.5 V from the lock-in amplifier's internal oscillator through a 250 kΩ resistor in series. The magnitude of the impedance between the source and drain can then be calculated. Figure 10 shows the impedance of the InN sample for different applied gate voltages.

In the model shown in the inset of Fig. 10, the capacitance near the gate-liquid interface is taken to be approximately 13 times greater than the channel-liquid capacitance. This ratio is justified by the substantial difference in the areas of the gate electrode and the channel, indicating that the majority of the potential will be distributed across the working electrode, i.e., the source and drain regions. Consequently, the need for a reference electrode is eliminated. The circuit model illustrated in the inset of Fig. 10 is used for impedance analysis. Notably, a satisfactory fit is achieved using this model up to 1 kHz, and the resulting values for capacitance per unit area and R_{IL} are detailed in Table II.

[1] Dario Daghero, F. Paolucci, Alessandro Sola, Mauro Tortello, G. A. Ummarino, M. Agosto, R. S. Gonnelli, Jijeesh R. Nair, and Claudio Gerbaldi, Large conductance modulation of gold thin films by huge charge injection via electrochemical gating, Phys. Rev. Lett. **108**, 066807 (2012).

[2] Rajiv Misra, Mitchell McCarthy, and Arthur F. Hebard, Electric field gating with ionic liquids, Appl. Phys. Lett. **90**, 052905 (2007).

[3] Yuji Nakagawa, Yuichi Kasahara, Takuya Nomoto, Ryotaro Arita, Tsutomu Nojima, and Yoshihiro Iwasa, Gate-controlled BCS-BEC crossover in a two-dimensional superconductor, Science **372**, 190 (2021).

[4] Trevor A. Petach, Menyoung Lee, Ryan C. Davis, Apurva Mehta, and David Goldhaber-Gordon, Mechanism for the large conductance modulation in electrolyte-gated thin gold films, Phys. Rev. B **90**, 081108 (2014).

[5] E. Piatti, D. Daghero, G. A. Ummarino, F. Laviano, J. R. Nair, R. Cristiano, A. Casaburi, C. Portesi, A. Sola, and R. S. Gonnelli, Control of bulk superconductivity in a BCS superconductor by surface charge doping via electrochemical gating, Phys. Rev. B **95**, 140501 (2017).

[6] K. Ueno, S. Nakamura, H. Shimotani, H. T. Yuan, N. Kimura, T. Nojima, Hayuyoshi Aoki, Y. Iwasa, and M. Kawasaki, Discovery of superconductivity in $KTaO_3$ by electrostatic carrier doping, Nat. Nanotechnol. **6**, 408 (2011).

[7] Hongtao Yuan, Hidekazu Shimotani, Jianting Ye, Sungjae Yoon, Hasniah Aliah, Atsushi Tsukazaki, Masashi Kawasaki, and Yoshihiro Iwasa, Electrostatic and electrochemical nature of liquid-gated electric-double-layer transistors based on oxide semiconductors, J. Am. Chem. Soc. **132**, 18402 (2010).

[8] K. Ueno, S. Nakamura, H. Shimotani, A. Ohtomo, N. Kimura, T. Nojima, H. Aoki, Y. Iwasa, and M. Kawasaki, Electric-field-induced superconductivity in an insulator, Nat. Mater. **7**, 855 (2008).

[9] Jeff Walter, Bryan Voigt, Ezra Day-Roberts, Kei Heltemes, Rafael M. Fernandes, Turan Birol, and Chris Leighton, Voltage-induced ferromagnetism in a diamagnet, Sci. Adv. **6**, eabb7721 (2020).

[10] R. A. Hein, J. W. Gibson, R. Mazelsky, R. C. Miller, and J. K. Hulm, Superconductivity in germanium telluride, Phys. Rev. Lett. **12**, 320 (1964).

[11] J. L. Smith and P. J. Stiles, Superconducting energy gap in semiconducting GeTe, J. Low Temp. Phys. **26**, 101 (1977).

[12] Etienne Bustarret, C. Marcenat, P. Achatz, J. Kačmarčik, F. Lévy, A. Huxley, L. Ortéga, E. Bourgeois, Xavier Blase, and D. Débarre *et al.*, Superconductivity in doped cubic silicon, Nature **444**, 465 (2006).

[13] E. A. Ekimov, V. A. Sidorov, E. D. Bauer, N. N. Mel'Nik, N. J. Curro, J. D. Thompson, and S. M. Stishov, Superconductivity in diamond, Nature **428**, 542 (2004).

[14] T. Inushima, N. Kato, Duncan Kennedy Maude, Hai Lu, W. J. Schaff, R. Tauk, Y. Meziani, S. Ruffenack, Olivier Briot, and Wojciech Knap *et al.*, Superconductivity of InN with a well defined Fermi surface, Phys. Status Solidi (b) **243**, 1679 (2006).

[15] T. Inushima, V. V. Vecksin, S. V. Ivanov, V. Y. Davydov, T. Sakon, and M. Motokawa, Anisotropic superconductivity of InN grown by molecular beam epitaxy on sapphire (0001), Phys. Status Solidi (b) **228**, 9 (2001).

[16] Naruhisa Miura, Hideaki Ishii, Akira Yamada, Makoto Konagai, Yasuyuki Yamauchi, and Akio Yamamoto, Anomalous electrical characteristics of epitaxial InN films having a high electron concentration at very low temperature, Jpn. J. Appl. Phys. **36**, L256 (1997).

[17] R. Meservey and P. M. Tedrow, Measurements of the kinetic inductance of superconducting linear structures, J. Appl. Phys. **40**, 2028 (1969).

[18] Aviv Glezer Moshe, Eli Farber, and Guy Deutscher, Granular superconductors for high kinetic inductance and low loss quantum devices, Appl. Phys. Lett. **117**, 062601 (2020).

[19] Giorgio Di Battista, Kin Chung Fong, Andrés Díez-Carlón, Kenji Watanabe, Takashi Taniguchi, and Dmitri K. Efetov, Infrared single-photon detection with superconducting magic-angle twisted bilayer graphene, Sci. Adv. **10**, eadp3725 (2024).

[20] Burm Baek, Adriana E. Lita, Varun Verma, and Sae Woo Nam, Superconducting a-W_xSi_{1-x} nanowire single-photon detector with saturated internal quantum efficiency from visible to 1850 nm, Appl. Phys. Lett. **98**, 251105 (2011).

[21] F. Marsili, V. B. Verma, J. A. Stern, S. Harrington, A. E. Lita, T. Gerrits, I. Vayshenker, B. Baek, M. D. Shaw, R. P. Mirin, and S. W. Nam, Detecting single infrared photons with 93% system efficiency, Nat. Photonics **7**, 210 (2013).

[22] V. B. Verma, R. Horansky, F. Marsili, J. A. Stern, M. D. Shaw, A. E. Lita, R. P. Mirin, and S. W. Nam, A four-pixel single-photon pulse-position array fabricated from WSi superconducting nanowire single-photon detectors, Appl. Phys. Lett. **104**, 051115 (2014).

[23] Hongtao Yuan, Hidekazu Shimotani, Atsushi Tsukazaki, Akira Ohtomo, Masashi Kawasaki, and Yoshihiro Iwasa, High-density carrier accumulation in ZnO field-effect transistors gated by electric double layers of ionic liquids, Adv. Funct. Mater. **19**, 1046 (2009).

[24] R. E. Glover III and M. D. Sherrill, Changes in superconducting critical temperature produced by electrostatic charging, Phys. Rev. Lett. **5**, 248 (1960).

[25] H. L. Stadler, Changing properties of metals by ferroelectric polarization charging, Phys. Rev. Lett. **14**, 979 (1965).

[26] Jiman Choi, R. Pradheesh, Hyungsang Kim, Hyunsik Im, Yonuk Chong, and Dong-Hun Chae, Electrical modulation of superconducting critical temperature in liquid-gated thin niobium films, Appl. Phys. Lett. **105**, 012601 (2014).

[27] Erik Piatti, Alessandro Sola, Dario Daghero, Giovanni A. Ummarino, Francesco Laviano, Jijeesh R. Nair, Claudio Gerbaldi, Roberto Cristiano, Alessandro Casaburi, and Renato S. Gonnelli, Superconducting transition temperature modulation in NbN via EDL gating, J. Supercond. Novel Magn. **29**, 587 (2016).

[28] S. P. Chockalingam, Madhavi Chand, John Jesudasan, Vikram Tripathi, and Pratap Raychaudhuri, Superconducting properties and Hall effect of epitaxial NbN thin films, Phys. Rev. B **77**, 214503 (2008).

[29] Buddhadeb Pal, Bhanu P. Joshi, Himadri Chakraborti, Aditya K. Jain, Barun K. Barick, Kankat Ghosh, Apurba Laha, Subhabrata Dhar, and Kantimay Das Gupta, in *AIP Conference Proceedings* (AIP Publishing, Melville, NY, 2018), Vol. 1942.

[30] R. E. Jones, K. M. Yu, S. X. Li, W Walukiewicz, J. W. Ager, E. E. Haller, H. Lu, and W. J. Schaff, Evidence for p-type doping of InN, Phys. Rev. Lett. **96**, 125505 (2006).

[31] Barun Kumar Barick, Nivedita Prasad, Rajendra Kumar Saroj, and Subhabrata Dhar, Structural and electronic properties of InN epitaxial layer grown on c-plane sapphire by chemical vapor deposition technique, J. Vac. Sci. Technol. A **34**, 051503 (2016).

[32] B. K. Barick, Rajendra Kumar Saroj, Nivedita Prasad, D. S. Sutar, and S. Dhar, Network of vertically c-oriented prismatic InN nanowalls grown on c-GaN/sapphire template by chemical vapor deposition technique, J. Cryst. Growth **490**, 104 (2018).

[33] Kankat Ghosh, Jaswant Singh Rathore, and Apurba Laha, Tuning the effective band gap and finding the optimal growth condition of InN thin films on GaN/sapphire substrates by plasma assisted molecular beam epitaxy technique, Superlattices Microstruct. **101**, 405 (2017).

[34] Kosmas Prassides, Superconductivity at the double, Nat. Nanotechnol. **6**, 400 (2011).

[35] Martin Sagmeister, Ulrich Brossmann, Stephan Landgraf, and Roland Würschum, Electrically tunable resistance of a metal, Phys. Rev. Lett. **96**, 156601 (2006).

[36] Yonatan Dubi, Yigal Meir, and Yshai Avishai, Nature of the superconductor–insulator transition in disordered superconductors, Nature **449**, 876 (2007).

[37] Amit Ghosal, Mohit Randeria, and Nandini Trivedi, Role of spatial amplitude fluctuations in highly disordered s-wave superconductors, Phys. Rev. Lett. **81**, 3940 (1998).

[38] Michael Tinkham, *Introduction to Superconductivity* (Courier Corporation, North Chelmsford, MA, 2004).

[39] Pierre-Gilles De Gennes, *Superconductivity of Metals and Alloys* (CRC Press, Boca Raton, FL, USA, 2018).

[40] W. L. McMillan, Transition temperature of strong-coupled superconductors, Phys. Rev. **167**, 331 (1968).

[41] V. Yu Davydov, V. V. Emtsev, I. N. Goncharuk, A. N. Smirnov, V. D. Petrikov, V. V. Mamutin, V. A. Vekshin, S. V. Ivanov, M. B. Smirnov, and T. Inushima, Experimental and theoretical studies of phonons in hexagonal InN, Appl. Phys. Lett. **75**, 3297 (1999).

[42] Yang Guo, Yan-Feng Zhang, Xin-Yu Bao, Tie-Zhu Han, Zhe Tang, Li-Xin Zhang, Wen-Guang Zhu, E. G. Wang, Qian Niu, and Z. Q. Qiu *et al.*, Superconductivity modulated by quantum size effects, Science **306**, 1915 (2004).

[43] N. R. Werthamer, E. F. Helfand, and P. C. Hohenberg, Temperature and purity dependence of the superconducting critical field, H_{c2}. III. Electron spin and spin-orbit effects, Phys. Rev. **147**, 295 (1966).

[44] E. Helfand and N. R. Werthamer, Temperature and purity dependence of the superconducting critical field, H_{c2}. II, Phys. Rev. **147**, 288 (1966).

[45] Himadri Chakraborti, Bhanu P. Joshi, Chanchal K. Barman, Aditya K. Jain, Buddhadeb Pal, Bikash C. Barik, Tanmay Maiti, Rüdiger Schott, Andreas D. Wieck, and M. J. N. V. Prasad *et al.*, Formation of tungsten carbide by focused ion beam process: A route to high magnetic field resilient patterned superconducting nanostructures, Appl. Phys. Lett. **120**, 132601 (2022).

[46] Loren D. Alegria, Charlotte G. L. Bøttcher, Andrew K. Saydjari, Andrew T. Pierce, Seung Hwan Lee, Shannon P. Harvey, Uri Vool, and Amir Yacoby, High-energy quasiparticle injection into mesoscopic superconductors, Nat. Nanotechnol. **16**, 404 (2021).

[47] Giorgio De Simoni, Federico Paolucci, Paolo Solinas, Elia Strambini, and Francesco Giazotto, Metallic supercurrent field-effect transistor, Nat. Nanotechnol. **13**, 802 (2018).

[48] Ilia Golokolenov, Andrew Guthrie, Sergey Kafanov, Yu A. Pashkin, and Viktor Tsepelin, On the origin of the controversial electrostatic field effect in superconductors, Nat. Commun. **12**, 2747 (2021).

[49] Federico Paolucci, Francesco Crisá, Giorgio De Simoni, Lennart Bours, Claudio Puglia, Elia Strambini, Stefano Roddaro, and Francesco Giazotto, Electrostatic field-driven supercurrent suppression in ionic-gated metallic superconducting nanotransistors, Nano Lett. **21**, 10309 (2021).

[50] Mirko Rocci, Giorgio De Simoni, Claudio Puglia, Davide Degli Esposti, Elia Strambini, Valentina Zannier, Lucia Sorba, and Francesco Giazotto, Gate-controlled suspended titanium nanobridge supercurrent transistor, ACS Nano **14**, 12621 (2020).

[51] Yu Saito, Yuichi Kasahara, Jianting Ye, Yoshihiro Iwasa, and Tsutomu Nojima, Metallic ground state in an ion-gated two-dimensional superconductor, Science **350**, 409 (2015).

[52] Yu Saito, Tsutomu Nojima, and Yoshihiro Iwasa, Highly crystalline 2D superconductors, Nat. Rev. Mater. **2**, 1 (2016).

[53] Xiaoxiang Xi, Helmuth Berger, László Forró, Jie Shan, and Kin Fai Mak, Gate tuning of electronic phase transitions in two-dimensional $NbSe_2$, Phys. Rev. Lett. **117**, 106801 (2016).

[54] Jt T. Ye, Yj J. Zhang, R. Akashi, Ms S. Bahramy, R. Arita, and Y. Iwasa, Superconducting dome in a gate-tuned band insulator, Science **338**, 1193 (2012).

[55] Takaya Sato, Gen Masuda, and Kentaro Takagi, Electrochemical properties of novel ionic liquids for electric double layer capacitor applications, Electrochim. Acta **49**, 3603 (2004).

[56] Bikash C. Barik, Himadri Chakraborti, Aditya K. Jain, Buddhadeb Pal, H. E. Beere, D. A. Ritchie, and K. Das Gupta, Low-frequency resistance fluctuations in an ionic-liquid-gated channel probed by cross-correlation noise spectroscopy, Phys. Rev. Appl. **22**, 044068 (2024).